NOVEL METAMATERIAL SURFACES FROM PERFECTLY CONDUCTING SUBWAVELENGTH CORRUGATIONS*

ROBERT LIPTON†, ANTHONY POLIZZI†, AND LOKENDRA THAKUR†

Abstract. Motivated by the numerical experiments carried out in [S. C. Yurt, A. Elfrgani, M. I. Fuks, K. Ilyenko, and E. Schamiloglu, *IEEE Trans. Plasma Sci.*, 44 (2016), pp. 1280–1286], we apply an asymptotic analysis to show that corrugated waveguides can be approximated by smooth cylindrical waveguides with an effective metamaterial surface impedance. We show that this approximation is in force when the period of the corrugations is subwavelength. Here the metamaterial delivers an effective anisotropic surface impedance and imparts novel dispersive effects on signals traveling inside the waveguide. These properties arise from the subwavelength resonances inside the corrugations. For sufficiently deep corrugations, the metamaterial waveguide predicts backward wave propagation. In this way we may understand backward wave propagation as a multiscale phenomenon resulting from local resonances inside subwavelength geometry. Our approach is well suited to numerical computation, and we provide a systematic investigation of the effect of corrugation geometry on wave dispersion, group velocity, and power flow.

Key words. metamaterials, dispersion diagram, negative dispersion, group and phase velocities, hybrid modes

AMS subject classifications. 35Q61, 78A50, 78M35, 78M40

DOI. 10.1137/16M109733X

1. Introduction. We examine wave propagation inside periodically corrugated cylindrical waveguides in which the outer walls are perfect conductors. This type of waveguide is well known in the microwave literature [4]. We show that the effects of the corrugation geometry are captured by modeling the corrugated wave guide as a smooth circular waveguide surrounded by a metamaterial surface when the period of the corrugation geometry is sufficiently small.

The corrugated waveguide is a cylindrical waveguide of infinite length with circular cross section having periodic variations in the radius. The minimum radius of the waveguide is r_m, the maximum radius is $r_m + h$, and the corrugation depth is h. The periodic variation of the boundary is contained within the annular domain $\{r \mid r_m \leq r \leq r_m + h\}$; see Figure 2(a). The period of the variation is denoted by d and will be taken small relative to the inner radius r_m, i.e., $d < r_m$. On the other hand, the depth h of the corrugation is *not* small, and the ratio of inner to outer radius $r_m/(r_m + h)$ can take any value in the interval $(0, 1]$. Here the width of the corrugation is the fraction of the period d where the radius r of the wave guide exceeds r_m. Infinitely thin corrugations are obtained in the limit when the waveguide has cross section of radius r_m except for an infinitesimally small fraction of the period where $r_m < r \leq r_m + h$; see Figure 3(d).

We begin with Maxwell's equations in the waveguide. Assuming a subwavelength scale of corrugations, we expand the electric and magnetic fields in the waveguide as

series in the period of the corrugations. Passing to the limit of vanishing period our analysis replaces Maxwell's equations in the corrugated waveguide by the Maxwell system posed inside a circular waveguide of fixed radius r_m. The fields in the leading order theory satisfy Maxwell's equations on a smooth circular cylinder, of radius r_m, but now with an effective surface impedance boundary condition; see Figure 2. In this way, subwavelength variations in waveguide geometry are manifested only in an effective impedance condition imposed on a simpler problem. We provide an explicit formula for the effective surface admittance $\mathcal{Y}_{ad}$ that shows it is determined by standing waves inside each corrugation; see section 3. The effective admittance is seen to change sign for frequencies on either side of any standing wave resonance frequency; see (36). The homogenized waveguide recovers trends seen in direct numerical simulation [14] and predicts the emergence of negative dispersion for sufficiently deep corrugations. It is well suited to the fast numerical computation of dispersion relations, group velocities, and power flow, given below in section 4.

1.1. Background, motivation, and main results. Our work is motivated by the study of backward wave propagation in corrugated waveguide structures, specifically the observation that waveguides with sufficiently deep corrugations support backward waves for wavelengths longer than the corrugation period; see [14]. Early on, this was discovered in a heuristic way and exploited in [2] for infinitely thin corrugations in cylindrical waveguides. This is further investigated in more recent work [5]. These works employ the so-called surface impedance method [2], [3] to waveguides with infinitely thin periodic corrugations with periods smaller than the wavelength of the propagating modes. For this case the corrugated waveguides are formally replaced by a smooth circular waveguide having a nonisotropic but uniform impedance.

In this paper we depart from the earlier work and show that it is possible to recover an effective surface impedance model directly from Maxwell's equations for subwavelength corrugations through a direct asymptotic analysis. We show an effective impedance is a purely subwavelength phenomenon and naturally arises without having to assume infinitely thin corrugations as in [2] and [5]. It is emphasized that unlike the effective impedance layer treated in [13], we do not assume that the corrugation depth is small relative to the radius of the waveguide. The finite size of the corrugation depth is necessary for understanding its effect on wave dispersion inside the waveguide. Our study unambiguously shows that the presence of negative group velocity hybrid modes is a multiscale phenomenon that is captured directly from Maxwell's equations using asymptotic analysis. It is found numerically that negative group velocity modes correspond to positive values of $i\mathcal{Y}_{ad}$ while positive group velocity modes correspond to negative values of $i\mathcal{Y}_{ad}$; see section 4. Changes in the sign of $i\mathcal{Y}_{ad}$ are shown to be caused by resonances generated inside the chambers $\{r \mid r_m, r \leq r_m + h\}$ associated with the corrugated boundary. The sign change is deduced from an explicit spectral representation formula for $\mathcal{Y}_{ad}$; see section 3 and formula (36). In this way we see that the corrugated boundary functions as a true metamaterial influencing dispersion at wavelengths longer than the period of the corrugations.

The asymptotic analysis and effective surface impedance developed here recover the special case of surface impedance associated with infinitely thin corrugations reported in the microwave literature in the mid-20th century; see Clarricoats and Saha [2]. Our analysis shows that more general corrugations result in different effective surface impedances. For a given subwavelength corrugation profile, our method is applied to compute dispersion relations, group velocities, and power flow within the

waveguide. In particular, we use our model to study the effect of the corrugation depth on a waveguide's ability to support backward waves. The results presented in section 4 strongly affirm the results of the numerical investigation [14] which points to the existence of metamaterial phenomena inside corrugated waveguides. This behavior is also corroborated in the recent work [5], which makes use of surface impedance formalism for infinitely thin corrugations developed in [2].

1.2. Approach. In this paper we develop two-scale asymptotic expansions [1], [11]. This method has been applied to problems involving rough interfaces and rough boundaries in [6], [8], [7]. We employ this approach to homogenize the rough surface of the waveguide when the period d of the corrugation goes to zero. Here the depth of the corrugations is kept fixed as the period is sent to zero. This together with the perfect conducting boundary condition allows us to recover an effective surface impedance that captures the resonance frequencies of local hybrid modes inside subwavelength corrugations; see (10) and (13)–(17). These resonances appear as poles in the effective surface admittance as seen in the formula (36). The surface admittance $\mathcal{Y}_{ad}$ is computed in Figures 7(a) to 11. The local resonances are seen to directly affect the dispersive properties of the waveguide through the leading order dispersion relation given by Propositions 1 and 2.

The paper is organized as follows: The physical model is presented in section 2. The method of two-scale expansion is described in subsection 2.1, subsection 2.2, and subsection 2.3. The general formulation of the leading order theory for time harmonic Maxwell's equations is presented in subsection 2.4. In subsection 2.5, we present the effective surface admittance/impedance associated with hybrid modes. The effect of local resonances on the effective admittance and wave dispersion is illustrated analytically and numerically in section 3, and the effect of corrugation depth is explored in section 4. The two-scale asymptotic derivation of the model is presented in Appendix A.

2. Model description. We assume a cylindrical waveguide of infinite length. The outer metallic shell of the waveguide has periodic corrugations with no azimuthal variation. The outer radius of the waveguide is $r_m + h$, and the corrugation depth is h. Hence, the region of the waveguide with subwavelength periodic variation is contained in the annular domain $\{r \mid r_m \leq r \leq r_m + h\}$; see Figure 1 for a plane view and Figure 2(a) for a cut-away view. The period of the corrugations is small relative to the inner radius r_m and given by d.
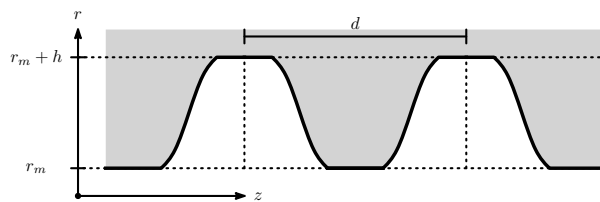

FIG. 1. *Truncated sinusoidal corrugations in annular domain* $\{r \mid r_m \leq r \leq r_m + h\}$ *of cylindrical waveguide.*

Examples of periodic corrugations include the d-periodic sinusoidal, saw tooth, and rectangular corrugations; see Figure 3. The corrugation shape is initially defined on a unit period, and the corrugations are described on rescaling by d. We define the corrugation profile through the shape function $\theta(r)$ defined for $r_m < r < r_m + h$; here $\theta(r) > 0$ and $|\theta'(r)| < \infty$; see Figure 4.

Within the waveguide, we assume a vacuum, while the surrounding metallic shell is treated as a perfect conductor. Thus, the electric and magnetic fields in the waveguide satisfy Maxwell's equations, satisfy perfectly conducting boundary conditions on the surface of the shell, and are zero within the thin conducting shell. Our asymptotic analysis results in the $d = 0$ surface impedance model in which periodic corrugations are replaced with an impedance surface surrounding the inner waveguide region $\{r \mid r \leq r_m\}$. Our effective surface impedance model is described in subsection 2.4 below and supports general propagating time-harmonic modes. The effective surface impedance model is also shown to support hybrid modes given by a mix of transverse electric (TE) and transverse magnetic (TM) fields. For this case we recover a more specific form of the effective surface impedance given in subsection 2.5.
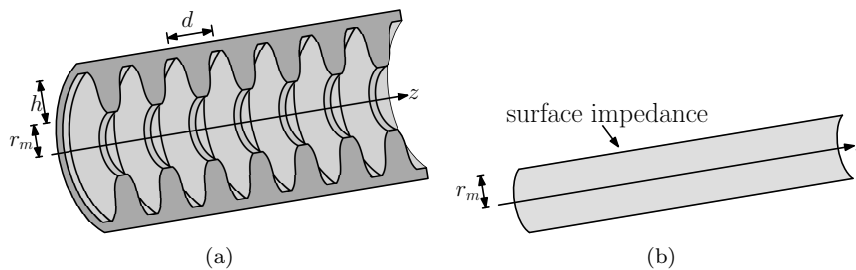

FIG. 2. (a) *Cut-away view of corrugated waveguide with d-periodic corrugations.* (b) *Homogenized limit given by waveguide of uniform circular cross section with effective surface impedance.*

2.1. Physics of waveguides and Maxwell's equations. In this paper, the periodic corrugation is represented by rescaling a unit-periodic geometry (see Figure 4) so that the corrugations are unit-periodic in $y = z/d$. The wavelength of a propagating mode is denoted by λ, and we are interested in subwavelength propagation, $d \ll \lambda$. The cylindrical waveguide has corrugated outer walls, and $\theta(r)$ denotes a profile function describing the corrugation shape as a function of r. In this paper, we investigate rectangular corrugation profiles [14] as well as sawtooth, sinusoidal, and infinitely thin rib profiles; see Figure 3.

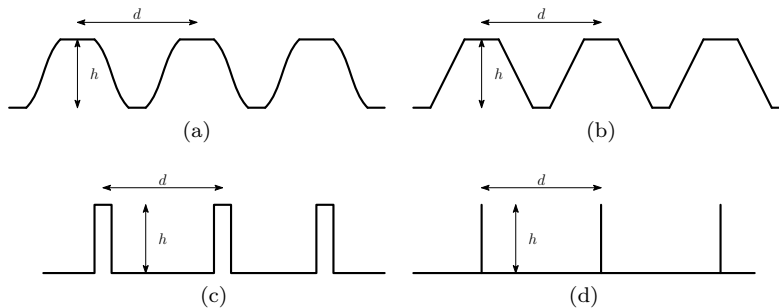FIG. 3. *Corrugation geometries considered:* (a) *Truncated sinusoidal corrugations;* (b) *truncated sawtooth corrugations;* (c) *rectangular corrugations;* (d) *infinitely thin corrugations.*

We assume that the electric and magnetic fields within the waveguide have the time-harmonic form

$$(1) \qquad \mathbf{E} = \mathbf{E}(y, z, r, \varphi)e^{i\omega t}, \qquad \mathbf{B} = \mathbf{B}(y, z, r, \varphi)e^{i\omega t},$$
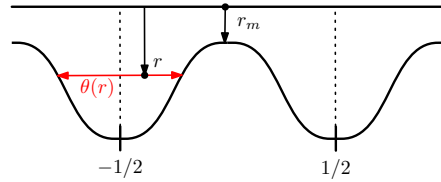
FIG. 4. *Unit-periodic geometry with unit-periodic corrugation and profile function $\theta(r)$.*

with $\mathbf{E}$ and $\mathbf{B}$ being unit-periodic in the "fast" y-variable, $y = z/d$. Here, (z, r, φ) denote canonical cylindrical coordinates. $\mathbf{E}$ and $\mathbf{B}$ exhibit both a d-periodic variation in z as well as a slow variation in z.

The waveguide is split into two concentric subdomains, denoted by Ω_W and Ω_I. Here, Ω_W is the cylindrical inner waveguide, $0 < r < r_m$; Ω_I is the region inside the corrugation, $r_m < r < r_m + h$ (see Figure 5).
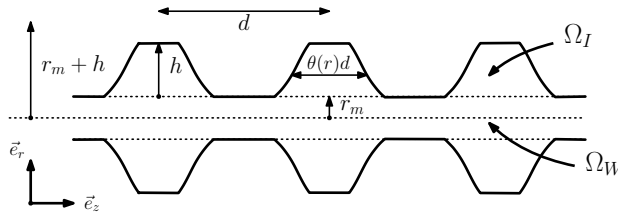

FIG. 5. *Plane view of domains Ω_I and Ω_W.*

The fields inside Ω_W are denoted by $\mathbf{E}^W, \mathbf{B}^W$, and the fields inside Ω_I are denoted by $\mathbf{E}^I, \mathbf{B}^I$. As we adopt $e^{i\omega t}$-time-harmonic behavior, on Ω_W, fields $\mathbf{E}^W, \mathbf{B}^W$ solve the time-harmonic Maxwell equations

$$(2) \qquad \begin{cases} \nabla \times \mathbf{E}^W = -i\omega \mathbf{B}^W, \\ \nabla \times \mathbf{B}^W = i\omega \mu_0 \epsilon_0 \mathbf{E}^W, \\ \nabla \cdot \mathbf{B}^W = 0, \\ \nabla \cdot \mathbf{E}^W = 0, \end{cases}$$

and $\mathbf{E}^I, \mathbf{B}^I$ satisfy, on Ω_I,

$$(3) \qquad \begin{cases} \nabla \times \mathbf{E}^I = -i\omega \mathbf{B}^I, \\ \nabla \times \mathbf{B}^I = i\omega \mu_0 \epsilon_0 \mathbf{E}^I, \\ \nabla \cdot \mathbf{B}^I = 0, \\ \nabla \cdot \mathbf{E}^I = 0. \end{cases}$$

On the outer boundary of the waveguide, denoting the unit outer normal vector field by $\vec{\nu}$, we impose perfect conducting boundary conditions

$$(4) \qquad \mathbf{E}^I \times \vec{\nu} = 0, \qquad \mathbf{B}^I \cdot \vec{\nu} = 0.$$

The waveguide boundary can have flat parts at $r = r_m$ for $y_-(r_m) < y < y_+(r_m)$; see Figure 5. Here we recall that the boundary of the waveguide is a metallic shell given by a perfect conductor with zero electric and magnetic fields inside. With this

in mind for $r = r_m$, we extend $\mathbf{E}^I$ and $\mathbf{B}^I$ by zero onto the flat parts. We write this observation as

$$(5) \qquad \begin{cases} \mathbf{E}^I(y, r_m, z, \varphi) = 0 \text{ for } y_-(r_m) < y < y_+(r_m), \\ \mathbf{B}^I(y, r_m, z, \varphi) = 0 \text{ for } y_-(r_m) < y < y_+(r_m). \end{cases}$$

With this extension we recover the continuity conditions at $r = r_m$ given by

$$(6) \qquad \begin{cases} (\mathbf{E}^W - \mathbf{E}^I) \times \vec{e}_r = 0, \\ (\mathbf{B}^W - \mathbf{B}^I) \cdot \vec{e}_r = 0. \end{cases}$$

We denote y-averages of a quantity q over the unit period $[-1/2, 1/2]$ by $\langle q \rangle = \int_{-1/2}^{1/2} q(y) dy$, and the homogenized transmission conditions at $r = r_m$ are

$$(7) \qquad \begin{cases} \langle \mathbf{B}^W - \mathbf{B}^I \rangle \times \vec{e}_r = \mathbf{J}(r, \varphi, z), \\ \langle \epsilon_0 \mathbf{E}^W - \epsilon_0 \mathbf{E}^I \rangle \cdot \vec{e}_r = \rho(r, \varphi, z). \end{cases}$$

Here $\mathbf{J}(r, \varphi, z)$ and $\rho(r, \varphi, z)$ are the homogenized surface current and charge density. The surface current and density are not prescribed but defined as the y-averages of the jumps in the electric and magnetic fields given on the left-hand side of (7).

2.2. Two-scale asymptotic expansions. As we are interested in subwavelength behavior, $d \ll \lambda$, we expand $\mathbf{E}^W, \mathbf{B}^W; \mathbf{E}^I, \mathbf{B}^I$ in the two-scale expansion

$$(8) \qquad \begin{cases} \mathbf{E}^W & = (\mathbf{E}^{W0}(y, z, r, \varphi) + d\mathbf{E}^{W1}(y, z, r, \varphi) + O(|d^2|))e^{i\omega t}, \\ \mathbf{B}^W & = (\mathbf{B}^{W0}(y, z, r, \varphi) + d\mathbf{B}^{W1}(y, z, r, \varphi) + O(|d^2|))e^{i\omega t}, \\ \mathbf{E}^I & = (\mathbf{E}^{I0}(y, z, r, \varphi) + d\mathbf{E}^{I1}(y, z, r, \varphi) + O(|d^2|))e^{i\omega t}, \\ \mathbf{B}^I & = (\mathbf{B}^{I0}(y, z, r, \varphi) + d\mathbf{B}^{I1}(y, z, r, \varphi) + O(|d^2|))e^{i\omega t}. \end{cases}$$

We substitute the series (8) into Maxwell's equations (2) and (3), perfect conducting boundary conditions (4), and transmission conditions (6) and (7) to recover the leading order theory describing propagating fields inside the waveguide. An outline of the derivation is provided in Appendix A. In the following, components of the electric and magnetic fields are written in cylindrical coordinates using the convention $\mathbf{E}^{W0} = (E_r^{W0}, E_z^{W0}, E_\varphi^{W0})$, $\mathbf{B}^{I0} = (B_r^{I0}, B_z^{I0}, B_\varphi^{I0})$, etc.

2.3. Leading order theory: The subwavelength limit of the asymptotic expansions. We present the boundary value problem for $\mathbf{E}^{W0}, \mathbf{B}^{W0}, \mathbf{E}^{I0}, \mathbf{B}^{I0}$. The derivation is given in Appendix A. In the interior waveguide, $0 < r < r_m$, the leading order fields $\mathbf{E}^{W0}, \mathbf{B}^{W0}$ are independent of the y variable, depending only on r, φ, z, and are solutions of Maxwell's equations

$$(9) \qquad \begin{cases} \nabla \times \mathbf{E}^{W0} & = -i\omega \mathbf{B}^{W0}, \\ \nabla \times \mathbf{B}^{W0} & = i\omega \mu_0 \epsilon_0 \mathbf{E}^{W0}, \\ \nabla \cdot \mathbf{B}^{W0} & = 0, \\ \nabla \cdot \mathbf{E}^{W0} & = 0. \end{cases}$$

Inside the impedance layer, $r_m < r < r_m + h$, the asymptotic analysis shows to leading order that the fields $\mathbf{E}^{I0}, \mathbf{B}^{I0}$ have the form

$$(10) \qquad \begin{cases} \mathbf{E}^{I0} & = \vec{e}_z E_z^{I0}, \\ \mathbf{B}^{I0} & = \vec{e}_\varphi B_\varphi^{I0} + \vec{e}_r B_r^{I0}, \end{cases}$$

and E_z^{I0}, B_φ^{I0}, B_r^{I0} are functions of r, φ, z. We emphasize that the polarization for $\mathbf{E}^{I0}$ and $\mathbf{B}^{I0}$ follows directly from the asymptotic analysis given in Appendix A and is not assumed. At the interface, $r = r_m$,

(11)
$$\begin{aligned} E_\varphi^{W0} &= 0, & E_z^{W0} &= E_z^{I0}, \\ -(B_\varphi^{W0} - \theta(r_m)B_\varphi^{I0}) &= J_z, & B_z^{W0} &= J_\varphi, \\ \epsilon_0 E_r^{W0} &= \rho, & B_r^{W0} &= B_r^{I0}, \end{aligned}$$

where ρ, J_z, and J_φ are surface charge densities and currents and are determined by the left-hand sides of (11). At $r = r_m + h$,

(12) $$B_r^{I0}(z, r_m + h, \varphi) = 0, \qquad E_z^{I0}(z, r_m + h, \varphi) = 0.$$

Here E_z^{I0}, B_φ^{I0}, B_r^{I0} satisfy the system

(13) $$\frac{1}{r}\partial_r\left(\frac{r}{\theta(r)}\partial_r(\theta E_z^{I0})\right) + \frac{1}{r^2}\partial_\varphi^2 E_z^{I0} = -\omega^2\mu_0\epsilon_0 E_z^{I0},$$

(14) $$E_z^{I0}(z, r_m + h, \varphi) = 0,$$

(15) $$B_r^{I0}(z, r_m + h, \varphi) = 0,$$

(16) $$B_r^{I0} = -\frac{1}{i\omega}\frac{1}{r}\partial_\varphi E_z^{I0},$$

(17) $$B_\varphi^{I0} = \frac{1}{i\omega\theta}\partial_r(\theta E_z^{I0}),$$

where (15) follows immediately from (16), noting that $\partial_\varphi E_z^{I0}$ is the tangential derivative on $r = r_m + h$ of E_z^{I0} and $E_z^{I0} = 0$ on $r = r_m + h$.

Taken together, (9)–(17) provide transmission and boundary conditions satisfied by $\mathbf{E}^{W0}$ and $\mathbf{B}^{W0}$ over the inner waveguide Ω_W. In the next section we consider solutions to the transmission boundary value problem for which the surface current J_z defined by the jump on the left-hand side of (11) vanishes. We subsequently find that such solutions exist by explicit construction. Assuming existence of solutions, it is possible to rewrite this problem as an equivalent one posed exclusively over Ω_W with an effective surface impedance boundary condition given on $r = r_m$.

2.4. Nonlocal surface impedance formulation for time-harmonic fields. We make the ansatz $\langle \mathbf{B}^W - \mathbf{B}^I \rangle \times \vec{e}_r = 0$, and a straightforward calculation gives $-(B_\varphi^{W0} - \theta(r_m)B_\varphi^{I0}) = 0$. With this ansatz we get $B_\varphi^{W0} = \theta(r_m)B_\varphi^{I0}$. We can now reinterpret the leading order theory for the time-harmonic electric and magnetic fields $\mathbf{E}^{W0}$ and $\mathbf{B}^{W0}$ as an equivalent problem defined on the circular waveguide Ω_W equipped with an effective anisotropic surface impedance. We now describe the equivalent problem on Ω_W and the effective surface impedance. In the domain $0 < r < r_m$, we have that the zero-order fields $\mathbf{E}^{W0}, \mathbf{B}^{W0}$ satisfy Maxwell's equations (9). Next we introduce the Dirichlet to Neumann map at the interface $r = r_m$. Define $F(r, \varphi)\vec{e}_z$ taking prescribed boundary data $f(\varphi)$ at $r = r_m$ and satisfying $F(r_m + h, \varphi) = 0$ and

(18) $$\frac{1}{r}\partial_r\left(\frac{r}{\theta(r)}\partial_r(\theta(r)F)\right) + \frac{1}{r^2}\partial_\varphi^2 F = -\omega^2\mu_0\epsilon_0 F$$

on $r_m < r < r_m + h$, $0 \leq \varphi \leq 2\pi$.

The Dirichlet to Neumann map for this problem, denoted by $\mathcal{N}_{\varphi,z}$, maps the Dirichlet data $F(r_m, \varphi) = f(\varphi)\vec{e}_z$ to the Neumann data $\frac{1}{i\omega}\partial_r(\theta F)_{|r_m}\vec{e}_\varphi$. At the

interface $r = r_m$, we impose (11) together with (13) and (14) to see that the anisotropic nonlocal surface impedance conditions are given on $r = r_m$ by

$$(19) \qquad E_\varphi^{W0}(r_m, \varphi, z) = 0, \qquad B_\varphi^{W0}(r_m, \varphi, z) = \mathcal{N}_{\varphi,z} E_z^{W0}(r_m, \varphi, z).$$

Collecting results, we obtain our fundamental result.

PROPOSITION 1 (periodic corrugations as metamaterials). *In the subwavelength limit $d \to 0$, a solution to the homogenized problem is given by the solution $(\mathbf{E}^{W0}, \mathbf{B}^{W0})$ of the time-harmonic Maxwell equations (9) in the circular waveguide Ω_W that satisfies the nonlocal anisotropic surface impedance conditions on the circular boundary $r = r_m$ of Ω_W given by (19).*

In the next section we apply this result to hybrid waveguide modes and recover explicit solutions to the homogenized problem posed in terms of the effective surface impedance.

2.5. Effective surface impedance for hybrid modes in circular waveguides. In this section we apply Proposition 1 to recover the leading order theory for waveguide modes inside the circular cylindrical waveguide. Waveguide modes inside the circular waveguide Ω_W have electric and magnetic fields according the following separated forms; see [2], [10]. In the interior waveguide, we have electric field

$$(20)$$
$$\mathbf{E}^{W0} = R_z^{En}(r)T_z^{En}(\varphi)e^{-i\beta z}\vec{e}_z + R_\varphi^{En}(r)T_\varphi^{En}(\varphi)e^{-i\beta z}\vec{e}_\varphi + R_r^{En}(r)T_r^{En}(\varphi)e^{-i\beta z}\vec{e}_r$$

and magnetic field

$$(21) \quad \mathbf{B}^{W0} = R_z^{Bn}(r)T_z^{Bn}(\varphi)e^{-i\beta z}\vec{e}_z + R_\varphi^{Bn}(r)T_\varphi^{Bn}(\varphi)e^{-i\beta z}\vec{e}_\varphi$$
$$+ R_r^{Bn}(r)T_r^{Bn}(\varphi)e^{-i\beta z}\vec{e}_r,$$

where the propagation constant $\beta = \frac{2\pi}{\lambda}$ and $n = 0, 1, 2, \ldots$. Here all functions $T(\varphi)$ of φ are of the form

$$(22) \qquad\qquad\qquad T(\varphi) = a_n e^{in\varphi},$$

where a_n is an arbitrary complex constant. We write $F(r, \varphi) = R(r)T(\varphi)$, and substitution of this form into (18) shows that $R(r)$ is the solution of

$$(23) \quad \begin{cases} r\frac{d}{dr}\left(\frac{r}{\theta(r)}\frac{d}{dr}(\theta(r)R(r))\right) + \left(r^2 k^2 - n^2\right)R(r) = 0, \ r_m < r < r_m + h, \\ R(r_m) = 1, \\ R(r_m + h) = 0, \end{cases}$$

where $k^2 = \omega^2/c^2$, $c = 1/\sqrt{\mu_0\epsilon_0}$, and μ_0 and ϵ_0 are the magnetic permeability and dielectric permittivity of the vacuum. From (19) we recover the anisotropic effective surface impedance conditions given by

$$(24) \qquad E_\varphi^{W0}(r_m, \varphi, z) = 0, \qquad B_\varphi^{W0}(r_m, \varphi, z) = \mu_0 \mathcal{Y}_{ad} E_z^{W0}(r_m, \varphi, z).$$

Here the surface impedance is expressed in terms of the effective admittance $\mathcal{Y}_{ad}$ given by

$$(25) \qquad\qquad \mathcal{Y}_{ad}(k, n) = \frac{y_0}{ik}\partial_r(\theta(r)R(r))\Big|_{r=r_m},$$

where $y_0 = \epsilon_0/\mu_0$ is the free space admittance. Collecting results, we find that subwavelength dispersion inside corrugated metallic waveguides is given to leading order by replacing the highly oscillatory corrugated boundary with a metamaterial having an anisotropic surface impedance.

PROPOSITION 2 (periodic corrugations as metamaterials II). *In the subwavelength limit $d \to 0$ all hybrid modes $(\mathbf{E}^{W0}, \mathbf{B}^{W0})$ are given by*

$$(26) \quad \begin{cases} E_z^{W0} = a_n J_n(x) e^{i(n\varphi - \beta z)}, \\ E_r^{W0} = -a_n i \frac{k}{K} \frac{J_n(x)}{x} \{\overline{\beta} F_n(x) + n\overline{\Lambda}\} e^{i(n\varphi - \beta z)}, \\ E_\varphi^{W0} = a_n \frac{k}{K} \frac{J_n(x)}{x} \{n\overline{\beta} + \overline{\Lambda} F_n(x)\} e^{i(n\varphi - \beta z)}, \\ B_z^{W0} = -a_n i c^{-1} \overline{\Lambda} J_n(x) e^{i(n\varphi - \beta z)}, \\ B_r^{W0} - a_n \frac{k}{K} c^{-1} \frac{J_n(x)}{x} \{\overline{\beta}\,\overline{\Lambda} F_n(x) + n\} e^{i(n\varphi - \beta z)}, \\ B_\varphi^{W0} = -a_n i \frac{k}{K} c^{-1} \frac{J_n(x)}{x} \{n\overline{\beta}\,\overline{\Lambda} + F_n(x)\} e^{i(n\varphi - \beta z)}, \ \ n = 0, 1, \dots, \end{cases}$$

where J_n is the Bessel function of order n, $x = Kr$, $K^2 = k^2 - \beta^2$, $\overline{\beta} = \beta/k$, $F_n(x) = x J_n'(x)/J_n(x)$, and the mode coupling parameter $\overline{\Lambda}$ is given by $-ic^{-1}\overline{\Lambda} = B_z^{WO}/E_z^{WO}$. All modes satisfy the anisotropic surface impedance conditions on the circular boundary $r = r_m$ of Ω_W given by (24) and $\mathcal{Y}_{ad}$ given by (25). The condition $E_\varphi^{W0}(r_m, \varphi, z) = 0$ specifies the coupling constant and for $x_m = Kr_m$ is given by

$$(27) \qquad\qquad\qquad n\overline{\beta} + \overline{\Lambda} F_n(x_m) = 0.$$

The condition $B_\varphi^{W0}(r_m, \varphi, z) = \mu_0 \mathcal{Y}_{ad} E_z^{W0}(r_m, \varphi, z)$ provides the k versus β dispersion relation for the waveguide modes given by

$$(28) \qquad\qquad \mu_0 \mathcal{Y}_{ad}(k, n) = -i \frac{k}{x_m K} \{n\overline{\beta}\,\overline{\Lambda} + F_n(x_m)\}.$$

For general corrugation shapes specified by $\theta(r)$ the admittance $\mathcal{Y}_{ad}(k, n)$ is computed through the numerical solution of (23). The dispersion relation is then solved for β at fixed k using a root finder in (28). For rectangular profiles $\theta(r)$ is a constant, (23) is a boundary value problem for Bessel's equation, and direct solution of (23) gives the explicit formula for the admittance

$$(29) \qquad \mathcal{Y}_{ad}(k, n) = -i \frac{\theta(r_m)}{c} \frac{Y_n(k(r_m + h)) J_n'(kr_m) - J_n(k(r_m + h)) Y_n'(kr_m)}{Y_n(k(r_m + h)) J_n(kr_m) - J_n(k(r_m + h)) Y_n(kr_m)}.$$

This formula shows that the effective admittance depends linearly on the relative width of the corrugation as well as its depth h. For $\theta = 1$ formula (29) recovers the surface impedance formula for corrugated waveguides with infinitely thin corrugations postulated in the early 1970s by Clarricoats and Saha [2]. This provides the connection between the metamaterial concept and the surface impedance formalism developed in the mid-20th century microwave literature.

We apply (28) to numerically examine the effect of corrugation depth and shape on dispersion curves in section 4.

3. Metamaterials and corrugations as microresonators. The characteristic feature of metamaterials is the coupling of macroscopic fields through structurally generated subwavelength resonance. For artificial magnetism generated in bulk metamaterials this is accomplished using split ring resonators made from perfect conductors as in [9]. For the metallic corrugated waveguides treated here, it is the finely

spaced corrugations that function as microresonators and provide the coupling between macroscopic electric and magnetic fields. Here the coupling is through the frequency-dependent effective surface admittance $\mathcal{Y}_{ad}$. We now provide an explicit formula for the effective admittance that explicitly highlights the effect of subwavelength resonances given by standing waves localized to the corrugations in the $d \to 0$ limit.

The standing waves are given for a fixed $n = 1, \ldots,$ by the orthonormal system $\{\phi_j^n(r)\}_{j=1}^{\infty}$ with respect to the weighted inner product $\langle u, v \rangle$ given by

$$(30) \qquad \langle u, v \rangle = \int_{r_m}^{r_m+h} u(r)v(r)p(r)\, dr,$$

where $p(r) = r/(\theta(r)) > 0$. Each standing wave ϕ_j^n and eigenvalue λ_j^n solve the Sturm–Liouville eigenvalue problem

$$(31) \qquad \frac{d}{dr}\left(p(r)\frac{d}{dr}\phi_j^n(r)\right) + t_n(r)\phi_j^n(r) = -\lambda_j^n p(r)\phi_j^n(r) \text{ for } r_m < r < r_m + h,$$

with $\phi_j^n(r_m) = \phi_j^n(r_m + h) = 0$ and $t_n(r) = -n^2/r\theta(r)$.

It is easily seen from (23) that the product $\phi(r) = \theta(r)R(r)$ is the solution of the boundary value problem

$$(32) \qquad \begin{cases} \frac{d}{dr}\left(p(r)\frac{d}{dr}\phi(r)\right) + \frac{(r^2k^2-n^2)}{r\theta(r)}\phi(r) = 0, \ r_m < r < r_m + h, \\ \phi(r_m) = \theta(r_m), \\ \phi(r_m + h) = 0, \end{cases}$$

and the admittance is written as

$$(33) \qquad \mathcal{Y}_{ad}(k, n) = \frac{y_0}{ik}\frac{d}{dr}\phi(r)|_{r=r_m}.$$

We can write $\phi(r) = v(r) + \ell(r)$, where $\ell(r) = \theta(r_m)(1 - (r - r_m)/h)$ and $v(r)$ is the solution of

$$(34) \qquad \begin{cases} \frac{d}{dr}\left(p(r)\frac{d}{dr}v(r)\right) + \frac{(r^2k^2-n^2)}{r\theta(r)}v(r) = g(r), \ r_m < r < r_m + h, \\ g(r) = \left(-\frac{d}{dr}\left(p(r)\frac{d}{dr}\ell(r)\right) - \frac{(r^2k^2-n^2)}{r\theta(r)}\ell(r)\right) \end{cases}$$

with the homogeneous boundary conditions $v(r_m) = v(r_m + h) = 0$.

We can express $v(x)$ for n fixed in terms of the standing waves $\{\phi_j^n\}_{j=1}^{\infty}$ as

$$(35) \qquad v(r) = \sum_{j=1}^{\infty} \frac{\langle g, \phi_j^n \rangle \phi_j(r)}{k^2 - (\lambda_j^n)},$$

and the spectral formula for the effective admittance is given by the following proposition.

PROPOSITION 3 (explicit spectral representation formula for the effective surface admittance).

$$(36) \qquad \mathcal{Y}_{ad}(k, n) = \frac{y_0}{ik}\left[-\frac{\theta(r_m)}{h} + \sum_{j=1}^{\infty} \frac{\langle g, \phi_j^n \rangle \frac{d}{dr}\phi_j^n(r)|_{r=r_m}}{k^2 - \lambda_j^n}\right].$$

The formula for the effective surface admittance shows that for a fixed azimuthal symmetry n the surface admittance changes sign for square frequencies k^2 in the range just below λ_j^n to just above it, where λ_j^n is the jth standing wave resonance.

For numerical simulation we measure corrugation depth in relative units as the ratio $r_m/(r_m + h)$, where smaller ratios correspond to deeper corrugations. The resonances of the surface admittance at a fixed frequency depend upon the depth of the corrugations. This is illustrated in Figures 6(a) and 6(b) for rectangular corrugations and truncated sinusoidal profiles, where the truncated sinusoidal profiles have the form

$$\theta(r) = \frac{1}{2} + \frac{1}{\pi} \arcsin[2(r - (r_m + h/2))/1.2h];$$

see Figure 3(a). The admittance is plotted as a function of frequency for fixed corrugation depths for rectangular, truncated sinusoidal, sawtooth, and infinitely thin corrugations in Figures 7(a) to 11. It is seen that the admittance changes sign and exhibits resonances at different frequencies for different corrugation profiles.
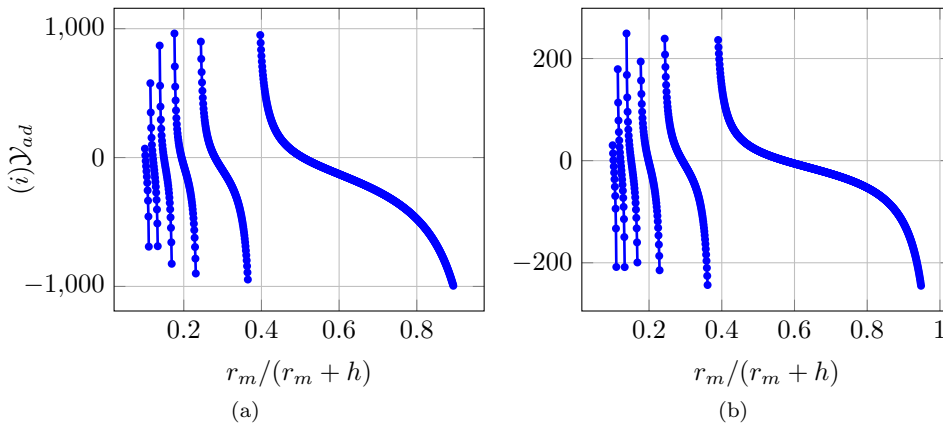

FIG. 6. *Admittance $\mathcal{Y}_{ad}$ as a function of corrugation depth ratio $r_m/(r_m + h)$ for (a) rectangular corrugations ($\theta \equiv 3/5$) and (b) truncated sinusoidal corrugations at fixed frequency $\omega \approx 50 \times 10^9$ rad/s, which corresponds to $kr_m = 2.0$.*

4. Controlling negative dispersion and power flow with corrugation depth. Backward waves are traveling wave modes with group velocity and phase velocity in opposing directions. In all cases the phase velocity is directed along the waveguide in the positive $\vec{e}_z$ direction. In this section we show existence of backward waves for corrugated waveguides when the corrugations are sufficiently deep. It is seen that group velocity and integrated power flow can be made opposite the phase velocity, depending on the depth of the corrugations. We also confirm that negative group velocity modes correspond to EH_{11} modes defined by $E_z > H_z$. This is important to describe Cherenkov interaction between the electromagnetic wave and electrons inside traveling wave tube amplifiers [14].

For future reference we will refer to the cut-off frequency for a dispersion curve as the frequency on the dispersion curve for which $\beta = 0$. Figures 12(a) to 13(b) give dispersion curves for hybrid modes and their dependence on the depth of corrugations. As before, depth is measured in relative units as the ratio $r_m/(r_m + h)$, and we consider corrugation depths associated with ratios between 0.3 and 0.6. The dispersion
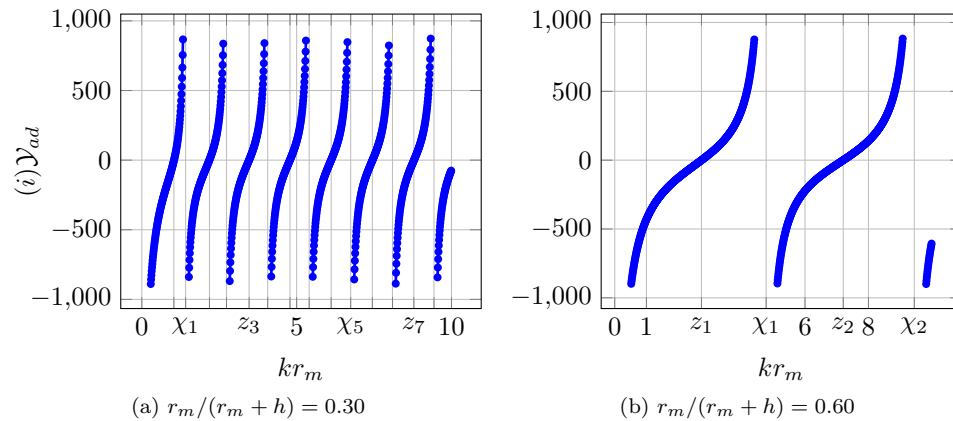
(a) $r_m/(r_m + h) = 0.30$ (b) $r_m/(r_m + h) = 0.60$

FIG. 7. (a) *Admittance* $\mathcal{Y}_{ad}$ *as a function of frequency for fixed ratio* $r_m/(r_m + h) = 0.30$ *with rectangular ribbed corrugations* ($\theta \equiv 3/5$). *Resonances are seen at frequencies where* kr_m *takes values of* $\chi_1 \approx 1.415$, $\chi_2 \approx 2.735$, $\chi_3 \approx 4.065$, $\chi_4 \approx 5.405$, $\chi_5 \approx 6.745$, $\chi_6 \approx 8.095$, $\chi_7 \approx 9.435$. *Zeros are seen at* $z_1 \approx 1.035$, $z_2 \approx 2.185$, $z_3 \approx 3.465$, $z_4 \approx 4.785$, $z_5 \approx 6.115$, $z_6 \approx 7.445$, $z_7 \approx 8.785$. (b) *Admittance* $\mathcal{Y}_{ad}$ *as a function of frequency for fixed ratio* $r_m/(r_m + h) = 0.60$ *with rectangular ribbed corrugations* ($\theta \equiv 3/5$). *Resonances are seen at frequencies where* kr_m *takes values of* $\chi_1 \approx 4.775$, $\chi_2 \approx 9.445$. *Zeros are seen at* $z_1 \approx 2.735$, $z_2 \approx 7.205$.

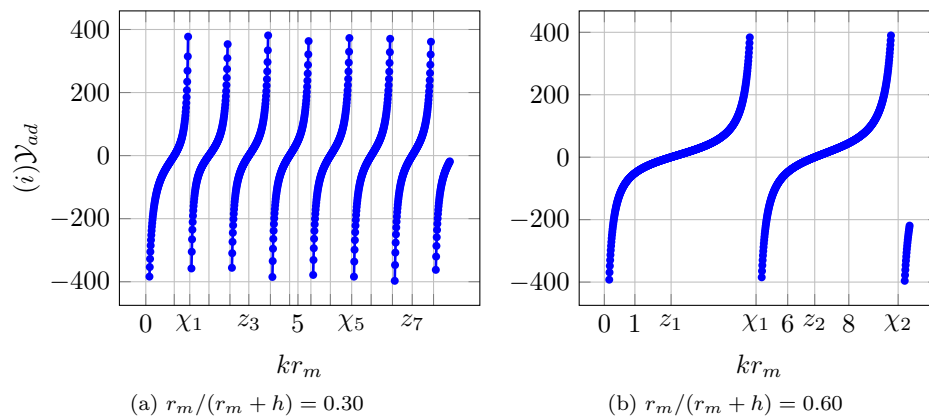(a) $r_m/(r_m + h) = 0.30$ (b) $r_m/(r_m + h) = 0.60$

FIG. 8. (a) *Admittance* $\mathcal{Y}_{ad}$ *as a function of frequency for fixed ratio* $r_m/(r_m + h) = 0.30$ *with truncated sinusoidal corrugations. Resonances are seen at frequencies where* kr_m *takes values of* $\chi_1 \approx 1.445$, $\chi_2 \approx 2.765$, $\chi_3 \approx 4.095$, $\chi_4 \approx 5.425$, $\chi_5 \approx 6.765$, $\chi_6 \approx 8.105$, $\chi_7 \approx 9.455$. *Zeros are seen at* $z_1 \approx 0.935$, $z_2 \approx 2.075$, $z_3 \approx 3.385$, $z_4 \approx 4.725$, $z_5 \approx 6.065$, $z_6 \approx 7.405$, $z_7 \approx 8.755$. (b) *Admittance* $\mathcal{Y}_{ad}$ *as a function of frequency for fixed ratio* $r_m/(r_m + h) = 0.60$ *with truncated sinusoidal corrugations. Resonances are seen at frequencies where* kr_m *takes values of* $\chi_1 \approx 4.965$, $\chi_2 \approx 9.615$. *Zeros are seen at* $z_1 \approx 2.185$, $z_2 \approx 6.885$.

relations are displayed in terms of normalized frequency and wave number given by kr_m and βr_m, respectively. For all cases we discover that there is a corrugation ratio below which all hybrid modes have backward waves associated with EH_{11} modes corresponding to $E_z > H_z$.

As a first example we consider rectangular corrugations of relative width $\theta(r_m) = 3/5$. Figure 12(a) shows a bifurcation between forward and backward wave modes for corrugation depth between the ratios of 0.6 and 0.48. The cut-off frequency for these
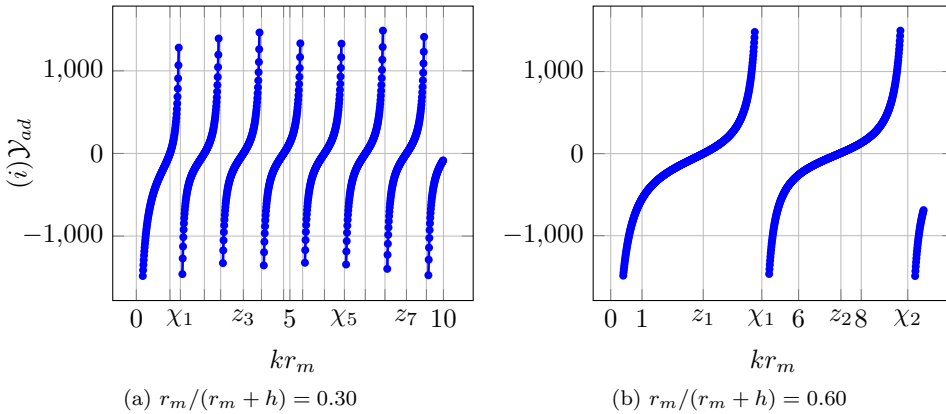
(a) $r_m/(r_m + h) = 0.30$ (b) $r_m/(r_m + h) = 0.60$

FIG. 9. (a) *Admittance* $\mathcal{Y}_{ad}$ *as a function of frequency for fixed ratio* $r_m/(r_m + h) = 0.30$ *with truncated sawtooth corrugations. The profile function* $\theta(r)$ *decreases linearly from* $\theta(r_m) = d_1 = 3/5$ *to* $\theta(r_m + h) = d_2 = 2/5$. *The slope of this profile then depends on the corrugation depth* h. *The profile function is given by* $\theta(r) = d_1 + ((d_2 - d_1)/h)(r - r_m)$. *Resonances are seen at frequencies where* kr_m *takes values of* $\chi_1 \approx 1.435$, $\chi_2 \approx 2.745$, $\chi_3 \approx 4.075$, $\chi_4 \approx 5.415$, $\chi_5 \approx 6.775$, $\chi_6 \approx 8.095$, $\chi_7 \approx 9.445$. *Zeros are seen at* $z_1 \approx 1.095$, $z_2 \approx 2.215$, $z_3 \approx 3.485$, $z_4 \approx 4.795$, $z_5 \approx 6.125$, $z_6 \approx 7.455$, $z_7 \approx 8.795$. (b) *Admittance* $\mathcal{Y}_{ad}$ *as a function of frequency for fixed ratio* $r_m/(r_m + h) = 0.60$ *with truncated sawtooth corrugations. Resonances are seen at frequencies where* kr_m *takes values of* $\chi_1 \approx 4.825$, $\chi_2 \approx 9.485$. *Zeros are seen at* $z_1 \approx 2.955$, $z_2 \approx 7.35$.

(a) $r_m/(r_m + h) = 0.30$ (b) $r_m/(r_m + h) = 0.60$

FIG. 10. (a) *Admittance* $\mathcal{Y}_{ad}$ *as a function of frequency for fixed ratio* $r_m/(r_m + h) = 0.30$ *with infinitely thin corrugations* ($\theta \equiv 1$). *Resonances are seen at frequencies where* kr_m *takes values of* $\chi_1 \approx 1.415$, $\chi_2 \approx 2.735$, $\chi_3 \approx 4.065$, $\chi_4 \approx 5.405$, $\chi_5 \approx 6.745$, $\chi_6 \approx 8.095$, $\chi_7 \approx 9.435$. *Zeros are seen at* $z_1 \approx 1.035$, $z_2 \approx 2.185$, $z_3 \approx 3.465$, $z_4 \approx 4.785$, $z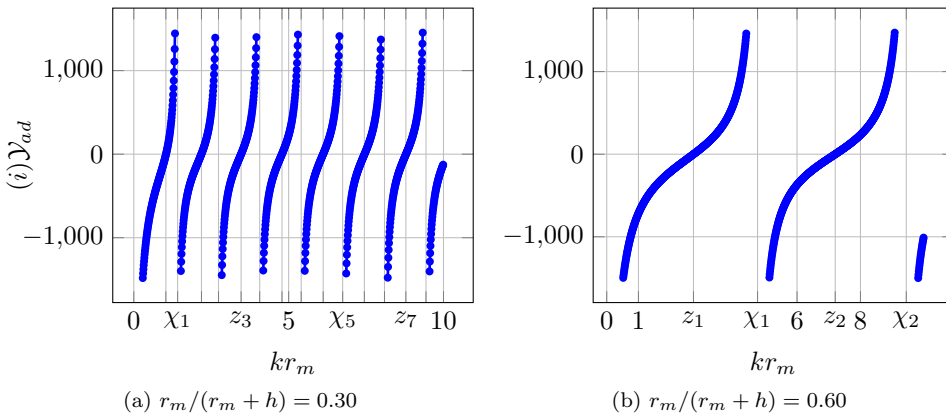_5 \approx 6.115$, $z_6 \approx 7.445$, $z_7 \approx 8.785$. (b) *Admittance* $\mathcal{Y}_{ad}$ *as a function of frequency for fixed ratio* $r_m/(r_m + h) = 0.60$ *with infinitely thin corrugations* ($\theta \equiv 1$). *Resonances are seen at frequencies where* kr_m *takes values of* $\chi_1 \approx 4.755$, $\chi_2 \approx 9.445$. *Zeros are seen at* $z_1 \approx 2.735$, $z_2 \approx 7.205$. *Note the poles and zeros for* $i\mathcal{Y}_{ad}$ *are the same for corrugations with* $\theta = 1$ *and* $\theta = 3/5$. *This follows from the explicit formula for* $i\mathcal{Y}_{ad}$ *given by* (29).

modes is approximately 1.8 in normalized units. The dispersion relation for the 0.48 corrugation exhibits negative group velocity at cut-off, while the mode associated with the 0.6 corrugation exhibits positive group velocity. The wave modes associated with deeper corrugations of ratios 0.4, 0.35, 0.3 are all EH_{11} modes and are backward waves
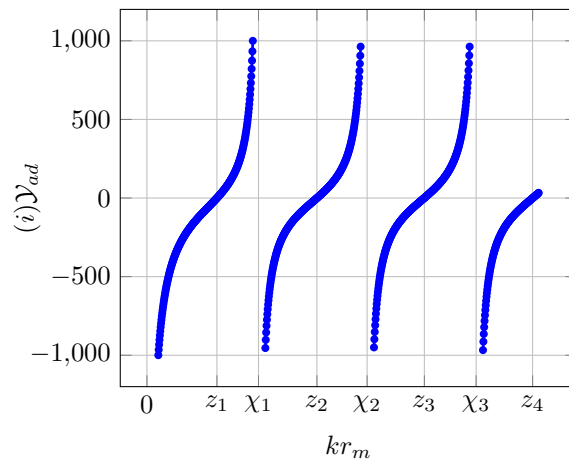
FIG. 11. *Admittance $\mathcal{Y}_{ad}$ as a function of frequency for the rectangular corrugations ($\theta \equiv 1/2$) considered in [14]. $r_m = 1.6$ cm, and $h = 1.8$ cm (this corresponds to depth ratio $r_m/(r_m + h) = 0.4706$). Resonances are seen at frequencies where kr_m takes values of $\chi_1 \approx 2.845$, $\chi_2 \approx 5.615$, $\chi_3 \approx 8.395$. Zeros are seen at $z_1 \approx 1.785$, $z_2 \approx 4.335$, $z_3 \approx 7.075$, $z_4 \approx 9.835$.*

exhibiting negative group velocity. For corrugations given by truncated sinusoidal profiles, Figure 12(b) shows similar trends. As seen before, there is a bifurcation between forward and backward wave modes for corrugation depth between the ratios of 0.6 and 0.48. The cut-off frequency for these modes is roughly 1.8 for the backward wave and 1.9 for the forward wave. As before, the dispersion relation for the 0.48 corrugation exhibits negative group velocity at cut-off, while the mode associated with the 0.6 corrugation exhibits positive group velocity. The wave modes associated with deeper corrugations of ratios 0.4, 0.35, 0.3 are also EH_{11} modes and are backward waves exhibiting negative group velocity. These trends are repeated for truncated sawtooth corrugations in Figure 13(a) and for the infinitely thin ribbed corrugations in Figure 13(b). We conclude by plotting dispersion relations for the rectangular corrugation geometries considered in [14]; see Figure 14(a). For this case, $r_m = 1.6$ cm, and we plot dispersion curves for ratios $r_m/(r_m + h)$ associated with different corrugation depths h. As before, we see a similar bifurcation between forward and backward modes in corrugated waveguides with increasing corrugation depth. We confirm existence of a backward wave EH_{11} mode at cut-off for a corrugation depth of 1.8 cm. In Figure 14(b) we plot both normalized group velocity $(dk/d\beta)/c$ and integrated Poynting vector $\int_0^{r_m} dP(r)$ for the rectangular corrugations of [14] (see Figure 14(a)) with corrugation depth $h = 1.8$ cm. We see that both are negative at the cut-off frequency and become positive for normalized wave numbers larger than 2.7. For comparison, we display Figure 15 associated with a positive wave for a rectangular corrugation with $\theta(r_m) = 3/5$ and a corrugation depth of ratio 0.6. Here both normalized group velocity and integrated Poynting vector are positive for all wave numbers on the dispersion curve.

We conclude this section by numerically demonstrating that negative group velocity modes correspond to positive values of $i\mathcal{Y}_{ad}$, while positive group velocity modes correspond to negative values of $i\mathcal{Y}_{ad}$; see section 4. Consider first rectangular corrugations with $\theta = 3/5$ with deep corrugations $r_m/(r_m + h) = 0.3$. Figure 7(a) shows $i\mathcal{Y}_{ad} > 0$ for normalized frequency between $z_1 = 1.035$ and $\chi_1 = 1.415$, and
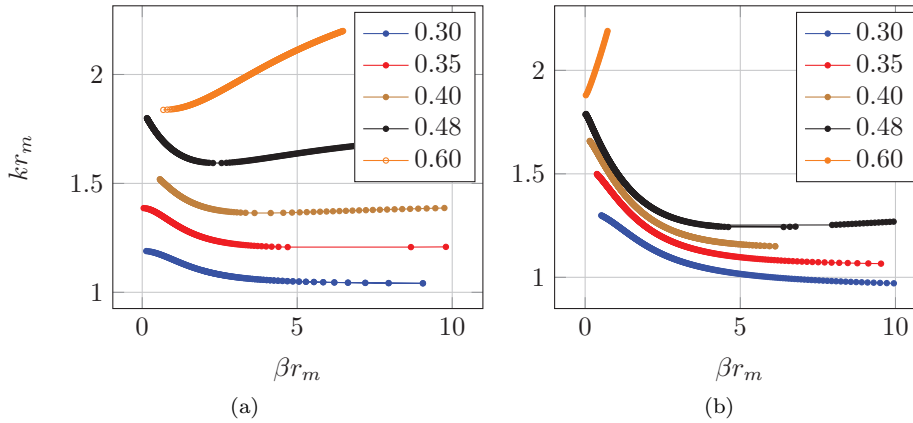
FIG. 12. (a) *Dispersion curves for rectangular corrugations with* $\theta \equiv 3/5$ *for corrugation depth ratios* $r_m/(r_m + h)$ *in the range* 0.3 *to* 0.6. (b) *Dispersion curves for truncated sinusoidal corrugations having the form* $\theta(r) = \frac{1}{2} + \frac{1}{\pi} \arcsin[2(r - (r_m + h/2))/1.2h]$ *for corrugation depth ratios* $r_m/(r_m + h)$ *in the range* 0.3 *to* 0.6.
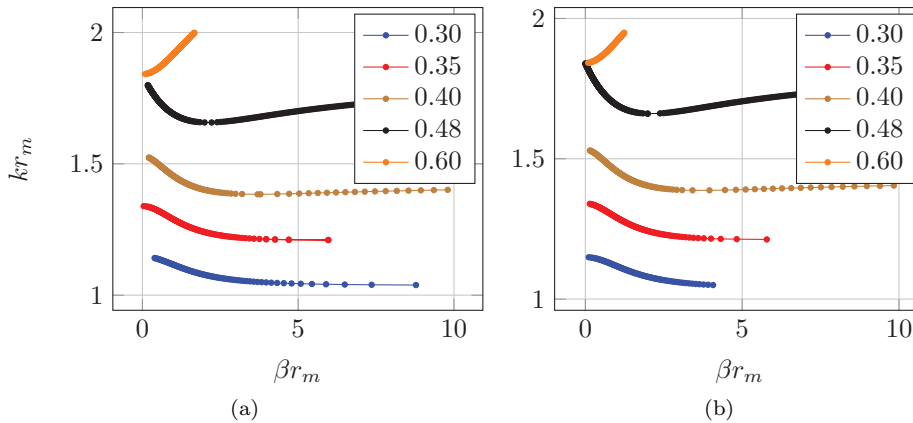

FIG. 13. (a) *Dispersion curves for truncated sawtooth corrugations. The profile function* $\theta(r)$ *decreases linearly from* $\theta(r_m) = d_1 = 3/5$ *to* $\theta(r_m + h) = d_2 = 2/5$. *The slope of this profile then depends on the corrugation depth* h. *The profile function is given by* $\theta(r) = d_1 + ((d_2 - d_1)/h)(r - r_m)$. *These are plotted for corrugation depth ratios* $r_m/(r_m + h)$ *in the range* 0.3 *to* 0.6. (b) *Dispersion curves for infinitely thin ribbed corrugations for corrugation depth ratios* $r_m/(r_m + h)$ *in the range* 0.3 *to* 0.6.

we see that this corresponds to the negative dispersion over that frequency range in the corresponding dispersion curve associated with $r_m/(r_m + h) = 0.3$ given in Figure 12(a). On the other hand, consider rectangular corrugations with $\theta = 3/5$ with shallow corrugations $r_m/(r_m + h) = 0.6$. Figure 7(b) shows $i\mathcal{Y}_{ad} < 0$ for normalized frequency less than $z_1 = 2.735$, and we see that this corresponds to the positive dispersion over that frequency range in the corresponding dispersion curve associated with $r_m/(r_m + h) = 0.6$ given in Figure 12(a).

This pattern is found to persist for all corrugation profiles. We now give a brief accounting. For truncated sinusoidal profiles with deep corrugations $r_m/(r_m + h) = 0.3$, Figure 8(a) shows $i\mathcal{Y}_{ad} > 0$ for normalized frequency between $z_1 = 0.935$ and $\chi_1 =$
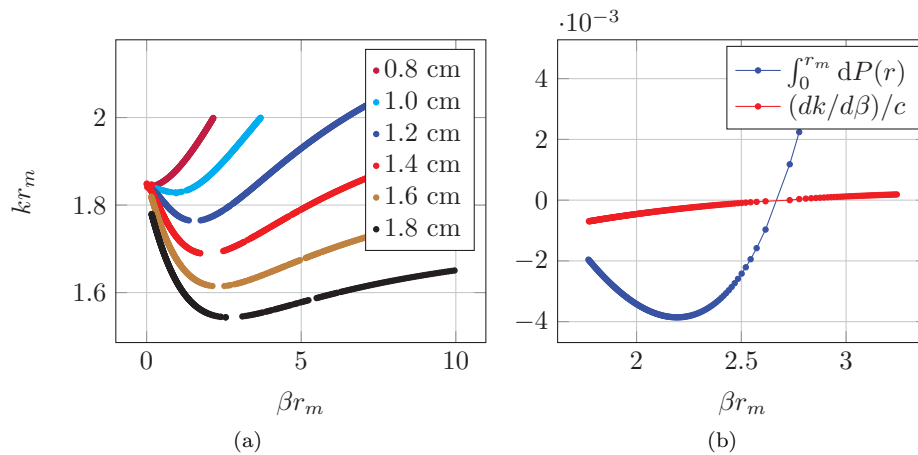
FIG. 14. (a) *Dispersion relation for the rectangular corrugations considered in* [14]. *Here an inner waveguide of radius* $r_m = 1.6$ *cm with rectangular corrugations* ($\theta \equiv 1/2$). *Dispersion relations are given for depths* $h = 0.8$ *cm* ($r_m/(r_m + h) \approx 0.667$), 1.0 *cm* ($r_m/(r_m + h) \approx 0.615$), 1.2 *cm* ($r_m/(r_m + h) \approx 0.5714$), 1.4 *cm* ($r_m/(r_m + h) \approx 0.5333$), 1.6 *cm* ($r_m/(r_m + h) = 0.5$), 1.8 *cm* ($r_m/(r_m + h) \approx 0.4706$). (b) *Normalized group velocity* $(dk/d\beta)/c$ *and integrated Poynting vector* $\int_0^{r_m} dP(r)$ *for the rectangular corrugations of* [14] *(see Figure* 14(a)) *with corrugation depth* $h = 1.8$ *cm (a ratio of* $r_m/(r_m + h) = 0.4706$).

1.445, and we see that this corresponds to the negative dispersion over that frequency range in the corresponding dispersion curve associated with $r_m/(r_m + h) = 0.3$ given in Figure 12(b). On the other hand, for shallow truncated sinusoidal corrugations $r_m/(r_m + h) = 0.6$, Figure 8(b) shows $i\mathcal{Y}_{ad} < 0$ for normalized frequency less than $z_1 = 2.185$, and this corresponds to the positive dispersion over that frequency range in the dispersion curve associated with $r_m/(r_m+h) = 0.6$ given in Figure 12(b). For truncated sawtooth profiles with deep corrugations $r_m/(r_m + h) = 0.3$, Figure 9(a) shows $i\mathcal{Y}_{ad} > 0$ for normalized frequency between $z_1 = 1.095$ and $\chi_1 = 1.435$, and we see that this corresponds to the negative dispersion over that frequency range in the corresponding dispersion curve associated with $r_m/(r_m + h) = 0.3$ given in Figure 13(a). On the other hand, for shallow truncated sawtooth corrugations $r_m/(r_m + h) = 0.6$, Figure 9(b) shows $i\mathcal{Y}_{ad} < 0$ for normalized frequency less than $z_1 = 2.955$, and this corresponds to the positive dispersion over that frequency range in the dispersion curve associated with $r_m/(r_m + h) = 0.6$ given in Figure 13(a). For infinitely thin but deep corrugations $r_m/(r_m + h) = 0.3$, Figure 10(a) shows $i\mathcal{Y}_{ad} > 0$ for normalized frequency between $z_1 = 1.035$ and $\chi_1 = 1.415$, and we see that this corresponds to the negative dispersion over that frequency range in the corresponding dispersion curve associated with $r_m/(r_m + h) = 0.3$ given in Figure 13(b). On the other hand, for shallow infinitely thin corrugations $r_m/(r_m + h) = 0.6$, Figure 10(b) shows $i\mathcal{Y}_{ad} < 0$ for normalized frequency less than $z_1 = 2.735$, and this corresponds to the positive dispersion over that frequency range in the dispersion curve associated with $r_m/(r_m + h) = 0.6$ given in Figure 13(b).

5. Conclusions. We have applied two-scale asymptotic expansions to confirm that negative group velocity can be induced through the design of subwavelength corrugations that are sufficiently deep. Our analysis and simulations definitively show that this phenomenon occurs due to the coupling of macroscopic electric and magnetic
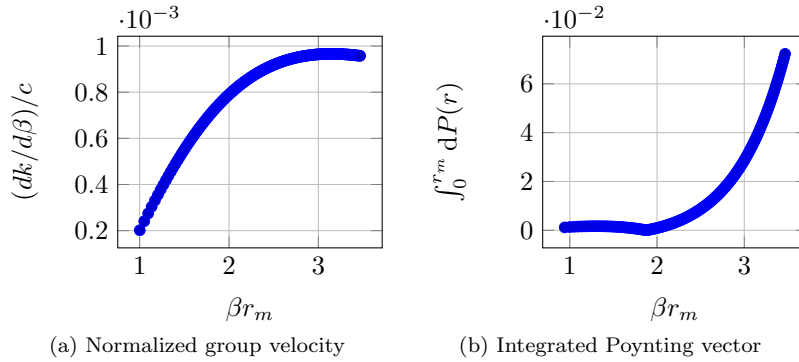
(a) Normalized group velocity   (b) Integrated Poynting vector

FIG. 15. *Normalized group velocity $(dk/d\beta)/c$ and integrated Poynting vector $\int_0^{r_m} dP(r)$ for the rectangular corrugations ($\theta \equiv 3/5$; see Figure 12(a)) with corrugation ratio $r_m/(r_m + h) = 0.6$. We observe that both the group velocity and the power flow are positive.*

fields through subwavelength resonance. This is manifested in an anisotropic effective surface impedance coupling electric to magnetic fields. The theory shows it is possible to represent corrugated waveguides as smooth cylindrical waveguides with a metamaterial surface characterized by an effective surface admittance. The effective surface admittance is the Dirichlet to Neumann map for a two point boundary value problem in terms of an ordinary differential equation with coefficients that depend on the corrugation shape. The interval over which the boundary value problem is posed depends upon the corrugation depth h and corresponds to the interval $r_m < r < r_m + h$. The reduced order model is far faster to compute than direct numerical simulation and can be used as a design tool for dispersion engineering. The reduced model allows one to quickly traverse the universe of geometries associated with corrugation profiles and depths. This enables fast prototyping of slow wave interaction structures for use in applications such as Cherenkov masers [12].

Appendix A. Derivation of the homogenized problem. In this section we derive the leading order transmission boundary value problem (9)–(17) using two-scale expansions.

A.1. Maxwell's equations in local coordinates. Again using the definition of the fast variable $y = z/d$ so that $\partial_z \to \partial_z + d^{-1}\partial_y$,

$$(37) \quad \begin{cases} \nabla\times\mathbf{E} &= \vec{e}_r(\frac{1}{r}\partial_\varphi E_z - (\partial_z + d^{-1}\partial_y)E_\varphi) \\ &\quad + \vec{e}_\varphi((\partial_z + d^{-1}\partial_y)E_r - \partial_r E_z) + \vec{e}_z(\frac{1}{r}\partial_r(rE_\varphi) - \frac{1}{r}\partial_\varphi E_r) \\ &= -i\omega(B_r\vec{e}_r + B_\varphi\vec{e}_\varphi + B_z\vec{e}_z), \\ \nabla\times\mathbf{B} &= \vec{e}_r(\frac{1}{r}\partial_\varphi B_z - (\partial_z + d^{-1}\partial_y)B_\varphi) \\ &\quad + \vec{e}_\varphi((\partial_z + d^{-1}\partial_y)B_r - \partial_r B_z) + (\frac{1}{r}\partial_r(rB_\varphi) - \frac{1}{r}\partial_\varphi B_r) \\ &= i\omega\mu_0\epsilon_0(E_r\vec{e}_r + E_\varphi\vec{e}_\varphi + E_z\vec{e}_z), \\ \nabla\cdot\mathbf{E} &= \frac{1}{r}\partial_r(rE_r) + \frac{1}{r}\partial_\varphi E_\varphi + (\partial_z + d^{-1}\partial_y)E_z = 0, \\ \nabla\cdot\mathbf{B} &= \frac{1}{r}\partial_r(rB_r) + \frac{1}{r}\partial_\varphi B_\varphi + (\partial_z + d^{-1}\partial_y)B_z = 0. \end{cases}$$

For $r_m < r < r_m + h$ the fast variable y lies in the waveguide between the corrugations. This is written as the union of intervals $-1/2 < y < y_-(r)$ and $y_+(r) < y < 1/2$, and this union is denoted by $Y(r)$. The width between corrugations $\theta(r)$ is

given by $\theta(r) = 1 - (y_+(r) - y_r(r))$. The interval $[-1/2, 1/2]$ is denoted by Y, and y values outside the waveguide are given by the interval $y_-(r) < y < y_+(r)$ or $Y \setminus Y(r)$ for $r_m < r < r_m + h$. The perfectly conducting boundary is $y = y_\pm(r)$. Part of the corrugations on $r = r_m$ can be flat sections of perfect conductor, and this corresponds to $y_-(r_m) < y < y_+(r_m)$ or $Y \setminus Y(r_m)$. Similarly, at $r = r_m + h$ there are flat parts, and this corresponds to $Y(r_m + h)$ given by the union $-1/2 < y < y_-(r_m + h)$ and $y_+(r_m + h) < y < 1/2$.

It is also convenient to write the boundary of the corrugation as a function of y. The boundary is written as $r = r_m + h(y)$, and recalling $y = x/d$, we get the formula for the normal vector to $y_\pm(r)$ given by

$$(38) \qquad \vec{\nu} = \frac{-d^{-1}\partial_y h(y)\vec{e}_z + \vec{e}_r}{(1 + d^{-2}(\partial_y h(y))^2)^{1/2}}.$$

For future reference, it is easily seen that

$$(39) \qquad \begin{cases} y'(r) & = \frac{1}{\partial_y h(y)}, \\ \theta'(r) & = y'_-(r) - y'_+(r). \end{cases}$$

With these preliminaries in hand, we describe boundary conditions on the waveguide boundary. On $y = y_\pm(r)$, $r_m < r < r_m + h$, the perfect conducting boundary conditions become

$$(40) \qquad \begin{cases} \vec{\nu} \cdot \mathbf{B}^I & = \frac{-d^{-1}\partial_y h(y)B_z^I + B_r^I}{(1 + d^{-2}(\partial_y h(y))^2)^{1/2}} = 0, \\ \vec{\nu} \times \mathbf{E}^I & = \frac{d^{-1}(\vec{e}_r \partial_y h E_\varphi^I - \vec{e}_\varphi \partial_y h E_r^I)}{(1 + d^{-2}(\partial_y h(y))^2)^{1/2}} + \vec{e}_z E_\varphi^I - \vec{e}_\varphi E_z^I = 0, \end{cases}$$

for $r = r_m$ and y on $Y \setminus Y(r_m)$

$$(41) \qquad \begin{cases} \vec{e}_r \times \mathbf{E}^W & = \vec{e}_z E_\varphi^W - \vec{e}_\varphi E_z^W = 0, \\ \vec{e}_r \cdot \mathbf{B}^W & = B_r^W = 0, \end{cases}$$

and for $r = r_m + h$ and y on $Y(r_m + h)$

$$(42) \qquad \begin{cases} \vec{e}_r \times \mathbf{E}^I & = \vec{e}_z E_\varphi^I - \vec{e}_\varphi E_z^I = 0, \\ \vec{e}_r \cdot \mathbf{B}^I & = B_r^I = 0. \end{cases}$$

We denote the operators ∇ and $\nabla\times$ expressed in terms of slow cylindrical variables r, φ, z by $\nabla_\mathbf{x}$ and $\nabla_\mathbf{x}\times$. Applying (37), for $\mathbf{E}$ and $\mathbf{B}$, denoting $\mathbf{E}^W, \mathbf{B}^W$ and $\mathbf{E}^I, \mathbf{B}^I$, we get the system

$$(43) \qquad \begin{cases} \nabla\times\mathbf{E} & = \nabla_\mathbf{x} \times \mathbf{E} + d^{-1}(-\vec{e}_r \partial_y E_\varphi + \vec{e}_\varphi \partial_y E_r) = -i\omega\mathbf{B}, \\ \nabla\times\mathbf{B} & = \nabla_\mathbf{x} \times \mathbf{B} + d^{-1}(-\vec{e}_r \partial_y B_\varphi + \vec{e}_\varphi \partial_y B_r) = i\omega\mu_0\epsilon_0\mathbf{E}, \\ \nabla \cdot \mathbf{E} & = \nabla_\mathbf{x} \cdot \mathbf{E} + d^{-1}\partial_y E_z = 0, \\ \nabla \cdot \mathbf{B} & = \nabla_\mathbf{x} \cdot \mathbf{B} + d^{-1}\partial_y B_z = 0. \end{cases}$$

In the next section we substitute the two-scale expansion into (5), (6), (7), and (40)–(43) and equate like powers of d to obtain a system of equations for determining the leading order theory.

A.2. Asymptotic theory. Substitution of expansions (8) into equations (40), (42), and (43) gives (for $\mathbf{E} = \mathbf{E}^W$ or $\mathbf{E} = \mathbf{E}^I$ and $\mathbf{B} = \mathbf{B}^W$ or $\mathbf{B} = \mathbf{B}^I$)

$$
(44\text{a}) \qquad \nabla_{\mathbf{x}} \times \mathbf{E}^{j-1} - \vec{e}_r \partial_y E_\varphi^j + \vec{e}_\varphi \partial_y E_r^j = -i\omega \mathbf{B}^{j-1},
$$

$$
(44\text{b}) \qquad \nabla_{\mathbf{x}} \times \mathbf{B}^{j-1} - \vec{e}_r \partial_y B_\varphi^j + \vec{e}_\varphi \partial_y B_r^j = i\omega \mu_0 \epsilon_0 \mathbf{E}^{j-1},
$$

$$
(44\text{c}) \qquad \nabla_{\mathbf{x}} \cdot \mathbf{E}^{j-1} + \partial_y E_z^j = 0,
$$

$$
(44\text{d}) \qquad \nabla_{\mathbf{x}} \cdot \mathbf{B}^{j-1} + \partial_y B_z^j = 0,
$$

and on $y = y_\pm(r)$,

$$
(45) \qquad \begin{cases} -\vec{e}_\varphi E_z^{I(j-1)} + \vec{e}_z E_\varphi^{I(j-1)} + \partial_y h(-\vec{e}_\varphi E_r^{Ij} + \vec{e}_r E_\varphi^{Ij}) = 0, \\ -\partial_y h B_z^{Ij} + B_r^{I(j-1)} = 0, \end{cases}
$$

and, at $r = r_m + h$ and y on $Y(r_m + h)$,

$$
(46) \qquad E_\varphi^{Ij} = 0, \qquad E_z^{Ij} = 0, \qquad B_r^{Ij} = 0.
$$

At $r = r_m$ and for $j = 0$, applying (6) and (7) gives

$$
(47) \qquad \begin{cases} -(E_\varphi^{W0} - E_\varphi^{I0})\vec{e}_z + (E_z^{W0} - E_z^{I0})\vec{e}_\varphi = 0, \\ -\langle B_\varphi^{W0} - B_\varphi^{I0}\rangle \vec{e}_z + \langle B_z^{W0} - B_z^{I0}\rangle \vec{e}_\varphi = J_z \vec{e}_z + J_\varphi \vec{e}_\varphi, \\ \langle \epsilon_0 E_r^{W0} - \epsilon_0 E_r^{I0}\rangle = \rho, \\ (B_r^{W0} - B_r^{I0}) = 0, \end{cases}
$$

and for $j > 0$,

$$
(48) \qquad \begin{cases} -(E_\varphi^{Wj} - E_\varphi^{Ij})\vec{e}_z + (E_z^{Wj} - E_z^{Ij})\vec{e}_\varphi = 0, \\ -\langle B_\varphi^{Wj} - B_\varphi^{Ij}\rangle \vec{e}_z + \langle B_z^{Wj} - B_z^{Ij}\rangle \vec{e}_\varphi = 0, \\ \langle \epsilon_0 E_r^{Wj} - \epsilon_0 E_r^{Ij}\rangle = 0, \\ (B_r^{Wj} - B_r^{Ij}) = 0, \end{cases}
$$

and from (5) and (41) for $r = r_m$ and y in $Y \setminus Y(r_m)$ and $j \geq 0$,

$$
(49) \qquad \begin{cases} \vec{e}_z E_\varphi^{Ij} - \vec{e}_\varphi E_z^{Ij} = 0, \\ B_r^{Ij} = 0, \end{cases}
$$

and

$$
(50) \qquad \begin{cases} \vec{e}_z E_\varphi^{Wj} - \vec{e}_\varphi E_z^{Wj} = 0, \\ B_r^{Wj} = 0. \end{cases}
$$

Here we use the convention that $\mathbf{E}^j, \mathbf{B}^j \equiv 0$ for $j < 0$.

A.3. $j = 0$ theory. The zero-order theory, i.e., (44a) with $j = 0$ gives

$$
(51) \qquad -\vec{e}_r \partial_y E_\varphi^0 + \vec{e}_\varphi \partial_y E_r^0 = 0,
$$

which holds for $\mathbf{E} = \mathbf{E}^{W0}$ and $\mathbf{E} = \mathbf{E}^{I0}$, while (44b) for $\mathbf{B}^{W0}$, $\mathbf{B}^{I0}$ yields

$$
(52) \qquad -\vec{e}_r \partial_y B_\varphi^0 + \vec{e}_\varphi \partial_y B_r^0 = 0.
$$

Equations (44c) and (44d) for both $\mathbf{B} = \mathbf{B}^{W0}, \mathbf{B}^{I0}$ and $\mathbf{E} = \mathbf{E}^{W0}, \mathbf{E}^{I0}$ yield

$$(53) \qquad \partial_y E_z^0 = 0, \qquad \partial_y B_z^0 = 0.$$

On the boundary, $y_\pm(r)$, $r_m < r < r_m + h$, we have

$$(54) \qquad -\vec{e}_\varphi E_r^{I0} + \vec{e}_r E_\varphi^{I0} = 0, \qquad -B_z^{I0} = 0,$$

so for y in Y and $0 < r < r_m$ and for y in $Y(r_m)$ and $r = r_m$,

$$(55) \qquad \begin{aligned} E_r^{W0} &= E_r^{W0}(z, r, \varphi), \quad E_z^{W0} = E_z^{W0}(z, r, \varphi), \quad E_\varphi^{W0} = E_\varphi^{W0}(z, r, \varphi), \\ B_r^{W0} &= B_r^{W0}(z, r, \varphi), \quad B_z^{W0} = B_z^{W0}(r, z, \varphi), \quad B_\varphi^{W0} = B_\varphi^{W0}(r, z, \varphi), \end{aligned}$$

and for y in $Y(r)$ and $r_m < r \leq r_m + h$,

$$(56) \qquad \begin{aligned} E_r^{I0} &= E_r^{I0}(z, r, \varphi), \quad E_z^{I0} = E_z^{I0}(z, r, \varphi), \quad E_\varphi^{I0} = E_\varphi^{I0}(z, r, \varphi), \\ B_r^{I0} &= B_r^{I0}(z, r, \varphi), \quad B_z^{I0} = B_z^{I0}(r, z, \varphi), \quad B_\varphi^{I0} = B_\varphi^{I0}(r, z, \varphi). \end{aligned}$$

Applying the boundary condition (54) shows that for $r_m < r \leq r_m + h$ and y in $Y(r)$,

$$(57) \qquad E_r^{I0}(z, r, \varphi) = 0, \qquad E_\varphi^{I0}(z, r, \varphi) = 0, \qquad B_z^{I0}(z, r, \varphi) = 0.$$

So, in the impedance layer $r_m < r < r_m + h$, y in $Y(r)$, we have

$$(58) \qquad \begin{cases} \mathbf{E}^{I0} &= \vec{e}_z E_z^{I0}(z, r, \varphi), \\ \mathbf{B}^{I0} &= \vec{e}_\varphi B_\varphi^{I0}(z, r, \varphi) + \vec{e}_r B_r^{I0}(z, r, \varphi), \end{cases}$$

with (from the boundary condition at $r = r_m + h$)

$$(59) \qquad \begin{cases} E_z^{I0}(z, r_m + h, \varphi) = 0, \\ B_r^{I0}(z, r_m + h, \varphi) = 0. \end{cases}$$

This establishes (10) and (12). The interface conditions at $r = r_m$ given by (11) now follow from a straightforward calculation using (5), (47), (49), (50), (55), (56), and (57). In the following section we recover the differential equations satisfied by the leading order theory.

A.4. $j = 1$ theory. In this final section we recover the differential equations (9), (13), (16), and (17) satisfied by $\mathbf{E}^{W0}$, $\mathbf{B}^{W0}$, $\mathbf{E}^{I0}$, and $\mathbf{B}^{I0}$. Starting with (44a) in both the interior waveguide and in the impedance layer, we have

$$(60) \qquad \nabla_{\mathbf{x}} \times \mathbf{E}^0 + (-\vec{e}_r \partial_y E_\varphi^1 + \vec{e}_\varphi \partial_y E_r^1) = -i\omega \mathbf{B}^0.$$

For $0 < r < r_m$ we integrate (60) in the y variable over Y and note that $\mathbf{E}^{W1}$ is periodic in y while $\mathbf{E}^{W0}$, $\mathbf{B}^{W0}$ are independent of y to recover the equation

$$(61) \qquad \nabla_{\mathbf{x}} \times \mathbf{E}^{W0} = -i\omega \mathbf{B}^{W0}, \qquad 0 < r < r_m.$$

For $r_m < r < r_m + h$, in the impedance layer, we integrate (60) over $-1/2 < y < y^-(r)$ and over $y^+(r) < y < 1/2$:

$$(62) \qquad \int_{-1/2}^{y^-(r)} \nabla_{\mathbf{x}} \times \mathbf{E}^{W0} \, dy + \left(-\vec{e}_r \int_{-1/2}^{y^-(r)} \partial_y E_\varphi^{W1} \, dy \right. $$
$$\left. + \vec{e}_\varphi \int_{-1/2}^{y^-(r)} \partial_y E_r^{W1} \, dy \right) = -i\omega \int_{-1/2}^{y^-(r)} \mathbf{B}^{W0} \, dy,$$

$$(63) \quad \int_{y^+(r)}^{1/2} \nabla_{\mathbf{x}} \times \mathbf{E}^{W0} \, \mathrm{d}y + \left(-\vec{e}_r \int_{y^+(r)}^{1/2} \partial_y E_\varphi^{W1} \, \mathrm{d}y \right.$$

$$\left. + \vec{e}_\varphi \int_{y^+(r)}^{1/2} \partial_y E_r^{W1} \, \mathrm{d}y \right) = -i\omega \int_{y^+(r)}^{1/2} \mathbf{B}^{W0} \, \mathrm{d}y.$$

We add (62) and (63), noting that $\mathbf{E}^{W0}$ and $\mathbf{B}^{W0}$ are independent of y, and apply

$$(64) \qquad \theta(r) = \int_{-1/2}^{y^-(r)} \mathrm{d}y + \int_{y^+(r)}^{1/2} \mathrm{d}y$$

to get

$$\theta(r)\nabla_{\mathbf{x}} \times \mathbf{E}^0 + \int_{y^+(r)}^{1/2} (-\vec{e}_r \partial_y E_\varphi^1 + \vec{e}_\varphi \partial_y E_r^1) \, \mathrm{d}y$$

$$+ \int_{-1/2}^{y^-(r)} (-\vec{e}_r \partial_y E_\varphi^1 + \vec{e}_\varphi \partial_y E_r^1) \, \mathrm{d}y = -i\omega\theta(r)\mathbf{B}^0.$$

Since $\mathbf{E}^{I1}$ is Y periodic, we get

$$(65) \quad \nabla_{\mathbf{x}} \times \mathbf{E}^{I0} + \theta^{-1}(r)(-\vec{e}_r(E_\varphi^1(y^-(r)) - E_\varphi^1(y^+(r)))$$

$$+ \vec{e}_\varphi(E_r^1(y^-(r)) - E_r^1(y^+(r)))) = -i\omega\mathbf{B}^{I0}.$$

From the boundary condition (45), for $r_m < r < r_m + h$, we deduce the scalar equations

$$(66) \qquad E_r^{I0}(y_\pm, z, r, \varphi) = -\frac{1}{\partial_y h(y_\pm)} E_z^{I0}(z, r, \varphi),$$

$$(67) \qquad E_\varphi^{I1}(y_\pm, z, r, \varphi) = 0,$$

and from earlier work, we have

$$E_\varphi^{I0}(z, r, \varphi) = 0, \qquad r_m < r < r_m + h.$$

Now, applying (39) and collecting results gives

$$(68) \qquad \vec{e}_\varphi(-\partial_r E_z^{I0} - \theta^{-1}(r)\partial_r \theta(r) E_z^{I0}) + \vec{e}_r\left(\frac{1}{r}\partial_\varphi E_z^{I0}\right) = -i\omega(\vec{e}_r B_r^{I0} + \vec{e}_\varphi B_\varphi^{I0})$$

for $r_m < r < r_m + h$. Taking the dot product of (68) with unit vector $\vec{e}_r$ in the impedance layer yields

$$(69) \qquad \frac{1}{r}\partial_\varphi E_z^{I0} = -i\omega B_r^{I0}, \quad r_m < r < r_m + h,$$

and the dot product of (68) with unit vector $\vec{e}_\varphi$ and elementary manipulation yields

$$(70) \qquad \partial_r(\theta(r)E_z^{I0}) = \theta(r)i\omega B_\varphi^{I0}, \quad r_m < r < r_m + h.$$

Apply (44b) with $j = 1$ for $0 < r < r_m$ to write

$$\nabla_{\mathbf{x}} \times \mathbf{B}^{W0} - \vec{e}_r \partial_y B_\varphi^{W1} + \vec{e}_\varphi \partial_y B_r^{W1} = i\omega\mu_0\epsilon_0 \mathbf{E}^{W0}.$$

As before, integrate both sides of this equation with respect to y over Y, noting that B_φ^{W1} and B_r^{W1} are periodic with respect to y and $\mathbf{B}^{W0}$ and $\mathbf{E}^{W0}$ are y independent to see that

$$(71) \qquad \nabla_{\mathbf{x}} \times \mathbf{B}^{W0} = i\omega\mu_0\epsilon_0\mathbf{E}^{W0}, \qquad 0 < r < r_m.$$

Inside the impedance layer $r_m < r < r_m + h$, the $j = 1$ theory for (44b) gives

$$\nabla_{\mathbf{x}} \times \mathbf{B}^{I0} - \vec{e}_r\partial_y B_\varphi^{I1} + \vec{e}_\varphi\partial_y B_r^{I1} = i\omega\mu_0\epsilon_0\mathbf{E}^{I0}.$$

Taking the dot product with $\vec{e}_z$ yields

$$(72) \qquad \frac{1}{r}\partial_r(rB_\varphi^{I0}) - \frac{1}{r}\partial_\varphi B_r^{I0} = i\omega\mu_0\epsilon_0 E_z^{I0}.$$

In the inner waveguide $0 < r < r_m$ the $j = 1$ theory for (44c) gives

$$\nabla_{\mathbf{x}} \cdot \mathbf{E}^{W0} + \partial_y E_z^{W1} = 0.$$

Again, integrating this equation over $y \in Y$ and using the y-periodicity of E_z^{W1} gives us

$$(73) \qquad \nabla_{\mathbf{x}} \cdot \mathbf{E}^{W0} = 0, \qquad 0 < r < r_m.$$

Similarly, we can apply (44d) to find

$$(74) \qquad \nabla_{\mathbf{x}} \cdot \mathbf{B}^{W0} = 0, \qquad 0 < r < r_m.$$

Now applying the $j = 1$ theory for (44d) inside the impedance layer $r_m < r < r_m + h$ we have

$$\nabla_{\mathbf{x}} \cdot \mathbf{B}^{I0} + \partial_y B_z^{I1} = 0.$$

Here, $\mathbf{B}^{I0} = \vec{e}_r B_r^{I0}(z,r,\varphi) + \vec{e}_\varphi B_\varphi^{I0}(z,r,\varphi)$, and, in local coordinates, we get

$$\frac{1}{r}\partial_r(rB_r^{I0}) + \frac{1}{r}\partial_\varphi B_\varphi^{I0} + \partial_y B_z^{I1} = 0.$$

At the boundaries $y_\pm(r)$, the $j = 1$ theory for (45) gives

$$(75) \qquad \partial_y h(y_\pm)B_z^{I1}(y_\pm(r),z,r,\varphi) = B_r^{I0}(z,r,\varphi),$$

and integrating (75) over $-1/2 < y < y_-(r)$ and $y_+(r) < y < 1/2$ (and adding the results) gives

$$(76) \quad \theta(r)\left(\frac{1}{r}\partial_r(rB_r^{I0}) + \frac{1}{r}\partial_\varphi B_\varphi^{I0}\right) + B_z(y^-(r),z,r,\varphi) - B_z^{I1}(-1/2,z,r,\varphi)$$
$$+ B_z^{I1}(1/2,z,r,\varphi) - B_z^{I1}(y^+(r),z,r,\varphi) = 0.$$

Applying (39) and (75) gives the string of equalities

$$B_z^{I1}(y_-(r),z,r,\varphi) - B_z^{I1}(y_+(r),z,r,\varphi) = \left(\frac{1}{\partial_y h(y_-)} - \frac{1}{\partial_y h(y_+)}\right)B_r^{I0}(z,r,\varphi)$$
$$= (\partial_r y_-(r) - \partial_r y_+(r))B_r^{I0}(z,r,\varphi)$$
$$= \partial_r \theta(r)B_r^{I0}(z,r,\varphi),$$

and we arrive at the equation

$$(77) \qquad \theta(r)\left(\frac{1}{r}\partial_r(rB_r^{I0}) + \frac{1}{r}\partial_\varphi B_\varphi^{I0}\right) + \partial_r\theta(r)B_r^{I0}(z, r, \varphi) = 0.$$

In summary, we have recovered (9) from (61), (71), (73), and (74). Equations (16) and (17) follow from (69) and (70). We then substitute (16) and (17) into (77) to see that (77) is satisfied identically. Finally, we recover (13) upon substituting (16) and (17) into (72).

Acknowledgments. The authors would like to thank E. Schamiloglu and S. Yurt from the University of New Mexico Department of Electrical & Computer Engineering for fruitful discussions and for sharing numerical experiments and expertise.

<div align="center">REFERENCES</div>

[1] A. Bensoussan, J. L. Lions, and G. Papanicolaou, *Asymptotic Analysis for Periodic Structures*, Stud. Math. Appl. 5, North–Holland, Amsterdam, 1978.

[2] P. J. B. Clarricoats and P. K. Saha, *Propagation and radiation behaviour of corrugated feeds. Part 1: Corrugated-waveguide feed*, Proc. Inst. Electrical Engineers, 118 (1971), pp. 1167–1176, https://doi.org/10.1049/piee.1971.0211.

[3] P. J. B. Clarricoats and M. I. Sobhy, *Propagation behaviour of periodically loaded waveguides*, Proc. Inst. Electrical Engineers, 115 (1968), pp. 652–651.

[4] J. L. Doane, *Propagation and mode coupling in corrugated and smooth-wall circular waveguides*, in Millimeter Components and Techniques Part IV, Infrared and Millimeter Waves 13, K. J. Button, ed., Academic Press, New York, 1985, pp. 123–170.

[5] E. García, J. Murphy, E. de Lera, and D. Segovia, *Analysis of the left-handed corrugated circular waveguide*, IET Microwaves Antennas Propagation, 2 (2008), pp. 659–667, https://doi.org/10.1049/iet-map:20070229.

[6] W. E. Kohler, G. C. Papanicolaou, and S. Varadhan, *Boundary and interface problems in regions with very rough boundaries*, in Multiple Scattering and Waves in Random Media, P. I. Chow, W. E. Kohler, and G. C. Papanicolaou, eds., North–Holland, Amsterdam, 1981, pp. 165–198.

[7] G. Kristensson, *Homogenization of corrugated interfaces in electromagnetics*, Progr. Electromagnetic Res., 55 (2005), pp. 1–31.

[8] J. Nevard and J. B. Keller, *Homogenization of rough boundaries and interfaces*, SIAM J. Appl. Math., 57 (1997), pp. 1660–1686, https://doi.org/10.1137/S0036139995291088.

[9] J. B. Pendry, J. A. Holden, J. D. Robbins, and W. J. Stewart, *Magnetism from conductors and enhanced nonlinear phenomena*, IEEE Trans. Microw. Theory Tech., 47 (1999), pp. 2075–2084.

[10] D. M. Pozar, *Microwave Engineering*, 2nd ed., John Wiley & Sons, New York, 1998.

[11] E. Sanchez-Palencia, *Non-homogeneous Media and Vibration Theory*, Lecture Notes in Phys. 127, Springer-Verlag, Berlin, 1980.

[12] L. Schächter, *Beam-Wave Interaction in Periodic and Quasi-periodic Structures*, Particle Accelerators and Detection, Springer-Verlag, Berlin, 1997.

[13] G. Stupakov and K. L. F. Bane, *Surface impedance formalism for a metallic beam pipe with small corrugations*, Phys. Rev. Accelerators Beams, 15 (2012), 124401, https://doi.org/10.1103/PhysRevSTAB.15.124401.

[14] S. C. Yurt, A. Elfrgani, M. I. Fuks, K. Ilyenko, and E. Schamiloglu, *Similarity of properties of metamaterial slow-wave structures and metallic periodic structures*, IEEE Trans. Plasma Sci., 44 (2016), pp. 1280–1286, https://doi.org/10.1109/TPS.2016.2535305.